Engineered Science
DOI: https://dx.doi.org/10.30919/es1646

Avoidance of Dead-Zone Formation in Flow-through Catalytic Membrane Reactor

Piotr Skrzypacz,[1] Qaiser Abbas,[2] Sławomir Szafert,[3] Vsevolod Andreev,[4] Askar Amirali[1] and Boris Golman[2,*]

Abstract

Nonlinear convection-diffusion-reaction equations play a vital role in chemical reactor engineering, particularly with the growing interest in the use of catalytic membrane reactors that require innovative numerical schemes. In this paper, a model is studied for a single reaction characterized by power-law kinetics that involves fractional reaction exponent. To address the challenge of dead-zone formation in a membrane with distributed catalyst due to the fractional reaction exponent, a suitable time-marching scheme is employed to solve the two-point nonlinear boundary value problem. A bisection algorithm is developed to effectively compute the necessary membrane velocity to suppress formation of dead zones. The effects of the Thiele modulus and reaction exponent on length of dead zone and its suppression are investigated. Through both analytical and numerical approaches, we provide valuable insights into the mechanisms underlying dead-zone formation and its mitigation strategies. These findings are useful for optimal design of membrane reactors and their operation.

Keywords: Flow-through catalytic membrane reactor; Dead zone suppression; Critical Thiele modulus; Nonlinear convection-diffusion-reaction equation; Time-marching scheme.
Received: 03 March 2025; Revised: 15 May 2025; Accepted: 29 May 2025
Type: Research article.

1. Introduction

Flow-through catalytic membrane reactors (FTCMR), which utilize catalyst-impregnated porous mem branes, have gained significant attention in various production processes due to their ability to enhance selectivity, minimize unwanted by-products, and reduce energy consumption.[1,2,3] These reactors have been successfully applied in hydrogen production, fine chemical synthesis, and environmental remediation.[1,4,5,6,7, 8,9] Such applications underline the versatility and scalability of FTCMR across chemical and environmental domains.

The concept of FTCMR delineates a novel approach to heterogeneous reactions, where the catalyst is immobilized within the pores of a predominantly ceramic membrane. These pores facilitate the movement of the reaction mixture through convection and diffusion.[10] The porous ceramic membrane acts solely as a microstructured catalyst support and does not perform any separation functions. By facilitating intensive contact between the catalyst and reactants while minimizing internal mass transport resistances, this type of reactor significantly improves the overall reaction rate.[11] Flow-through membrane reactors have demonstrated their effectiveness in numerous applications, including the partial hydrogenation of unsaturated substrates,[2] partial oxidation of propylene to form propylene oxide,[12] dimerization of isobutene into isooctane,[13] the thermal oxidation of dimethyl methylphosphonate (DMMP),[3] methane partial oxidation to produce formaldehyde,[14] synthesis of biodiesel via esterification reactions,[15] partial hydrogenation of 1,5-cyclooctadiene,[16] degradation of waterborne environmental contaminants,[17,18,19] catalytic reduction of nitrates/nitrites in water and dechlorination of chlorinated hydrocarbons.[20]

The formation of *dead zones*, *i.e.*, regions within the membrane where chemical reactions cease due to the depletion of reactants, is one of challenges in chemical reactor engineering. Numerous key catalytic reactions in industrial processes follow kinetics of power-law type with fractional reaction exponents.[21,22,23] The term *dead zone* was coined by Temkin[24] and has been widely adopted in the literature.[25,23,26,27] Such phenomena can negatively impact the reactor efficiency and have been observed in various applications, including the hydrogenation of propylene using commercially available catalysts,[23] the production of electricity in microbial fuel cells,[28] and bioreactions in catalytic particles containing immobilized enzymes.[29] In

[1]*School of Sciences and Humanities, Nazarbayev University, 53 Kabanbay Batyr Ave., Astana, 010000, Kazakhstan*
[2]*School of Engineering and Digital Sciences, Nazarbayev University, 53 Kabanbay Batyr Ave., Astana, 010000, Kazakhstan*

order to maximize the performance of flow-through reactors with catalytic membrane, it is essential to understand and mitigate the presence of dead zones in advance. Reducing or eliminating these inactive regions ensures more uniform reactant distribution, improved selectivity, and enhanced productivity.[1,30,31]

However, despite these technological advances, kinetic modeling in FTCMR remains a limiting factor in accurately capturing their performance. In practice, many catalytic processes exhibit fractional-order kinetics. For instance, Menaka *et al*.[32] investigated dead-core formation in non-isothermal catalyst pellets, while Skrzypacz *et al*.[27] developed semi-analytic solutions for dead zones under power-law kinetics with external mass transfer resistance. Haider *et al*.[33] and Kumar *et al*.[34] applied fractional derivatives to model transport and reaction in porous and thermal systems, effectively capturing memory effects and long-range interactions. Naeem *et al*.[35] presented exact solutions for time-fractional convection-reaction diffusion equations, demonstrating convergence with classical models. Additionally, Kazbek *et al*.[36] showed that non-uniform catalyst activity combined with periodic operation can enhance the performance of pellets governed by Langmuir-Hinshelwood kinetics. Nevertheless, the integration of fractional-order kinetics with convection-diffusion transport in FTCMR has yet to be thoroughly investigated. This leaves an important gap in the modeling of FTCMR, especially in conditions where reactant depletion can result in dead zones within the reactor.

In light of this, the primary objective of this paper is to suppress the formation of dead zones in flow through reactors with catalytic membrane by inducing additional convective transport within the membrane.

In order to effectively model and predict the formation of dead zones, researchers commonly utilize the concept of the critical Thiele modulus.[25,37] The Thiele modulus is a dimensionless process parameter that characterizes the relative rates of reaction and diffusion within a porous catalyst. It serves as a fundamental parameter in the design and analysis of catalytic membrane reactors. Dead zones form when the Thiele modulus surpasses its critical value.[25] Numerous studies have explored the formation of dead zones. For instance, the study in[38] investigated the formation of dead zones in porous catalysts under non-isothermal conditions with temperature-dependent diffusivity. Aris[37] developed solutions for both dead-core and non dead-core scenarios in pellets of planar geometry, excluding the effects of external mass transfer. Andreev[25] identified the necessary conditions for the formation of dead zones and calculated the critical Thiele modulus for spherical and cylindrical pellets, considering external mass transfer. Additionally, the formation of dead zones in slightly non-isothermal reactions was investigated in.[39] While extensive research has been conducted on dead-zone formation in catalytic slabs, particularly with power-law reaction kinetics, the literature concerning the formation of dead zones in flow-through reactors with catalytic membrane remains limited. This gap highlights the importance of our study, which aims to enhance the understanding of and provide solutions for mitigating dead-zone formation in these reactors. Simulations of dead-zone problems are challenging due to the non-differentiable nature of the reaction term at vanishing concentrations, which can lead to convergence issues for standard solvers. Existing numerical methods from the literature, such as those in,[40,41,42,43,44,45] often struggle with efficiency when applied to dead-zone problems. To address this challenge, we employ a modified Crank-Nicolson scheme, previously introduced in our works,[46,30] to efficiently solve the nonlinear steady-state problem for reactions characterized by power-law kinetics and fractional reaction exponents. For problems without dead-zone formation, standard numerical solvers or Taylor expansion methods (*e.g*.,[47]) can be used.

The remainder of this paper is organized as follows. Section 2 describes and analyzes the mathematical model governing transport processes within the catalytic membrane of the flow-through reactor. Section 3 addresses dead-core solutions for problems involving fractional reaction exponents and vanishing convection. For cases with non-vanishing convection, analytical solutions are generally not feasible unless the reaction exponent is zero. In that special case, a closed-form solution is derived, along with expressions for the critical Thiele modulus and the length of the dead zone. Section 4 introduces the time-marching numerical scheme for solving dead-core problems with non-vanishing convection. Section 5 presents the core methodological contribution of this work: a bisection algorithm developed to suppress dead-zone formation in catalytic membrane reactors. Section 6 provides numerical results that validate the time-marching scheme and bisection algorithm through simulations conducted across a range of model and process parameters. Finally, Section 7 presents concluding remarks.

2. Mathematical model

In the following, we investigate a one-dimensional model of a flow-through catalytic membrane reactor where reactant A is converted to the product within the porous membrane containing immobilized catalysts. As illustrated in Fig. 1, the catalytic membrane is closed at one end and the reactant A is introduced through the other open end. Upon entering the reactor, the reactant is forced to flow through the membrane, where the catalytic reaction occurs, converting A into the product. The unreacted portion of A, along with the product, exits the reactor through the opposite end. Given that the membrane's diameter is significantly larger than its thickness

[3]*Department of Chemistry, University of Wrocław, 14 F. Joliot-Curie, Wrocław, Lower Silesian Voivodeship, 50-383, Poland*
[4]*Department of Heat Power Setups, Faculty of Energy and Electrical Engineering, Chuvash State University, Cheboksary 428015, Russia*
**Email:* boris.golman@nu.edu.kz (Boris Golman)

L, a one-dimensional slab geometry is adopted for the model, simplifying the analysis. In this work, the case of a single reaction

$$A \rightarrow Products$$

is considered with kinetics of power-law type with fractional reaction exponent.

Table 1: Model parameters and variables.

Model parameters and variables	Units	Description
φ	$[-]$	Thiele modulus
Pe_m	$[-]$	mass Peclet number
C_A	$[mol \cdot m^{-3}]$	concentration of reactant A inside membrane
$C_{A,0}$	$[mol \cdot m^{-3}]$	concentration for reactant A in feed stream
$D_{A,\text{eff}}$	$[m^2 \cdot s^{-1}]$	effective diffusivity of component A
k	$[s^{-1}(mol/m^3)^{1-p}]$	preexponential constant of component A
p	$[-]$	reaction exponent
u_D	$[m \cdot s^{-1}]$	Darcian fluid velocity within the porous membrane
L	$[m]$	membrane thickness
x	$[m]$	distance variable
c	$[-]$	dimensionless concentration of component A
z	$[-]$	dimensionless distance variable

The concentration of reactant A within the catalytic membrane obeys the following two-point boundary value problem

$$\begin{aligned} -D_{A,\text{eff}}\frac{d^2C_A}{dx^2} + u_D\frac{dC_A}{dx} + kC_A^p = 0 \quad \text{in } (0,L), \\ C_A(0) = C_{A,0}, \\ \frac{dC_A}{dx}(L) = 0, \end{aligned} \tag{1}$$

where the model parameters and variables are presented in Table 1. After introducing dimensionless concentration $c = \frac{C_A}{C_{A,0}}$ and dimensionless distance $z = \frac{x}{L}$, Eq. (1) becomes

$$\frac{d^2c}{dz^2} - Pe_m\frac{dc}{dz} - \varphi^2c^p = 0 \quad \text{in } (0,1), \tag{2}$$

subject to the boundary conditions

$$c(0) = 1 \quad \text{and} \quad \frac{dc}{dz}(1) = 0. \tag{3}$$

The dimensionless parameters in Eq. (2) are defined as

$$\varphi = \sqrt{\frac{L^2 \cdot k \cdot C_{A,0}^{p-1}}{D_{A,\text{eff}}}} \quad \text{and} \quad Pe_m = \frac{L \cdot u_D}{D_{A,\text{eff}}}, \tag{4}$$

representing the Thiele modulus and mass Peclet number, respectively.

Remark 1. The model equation for the cylindrical geometry is expressed as[30]:

$$\frac{d^2c}{dz^2} + \left(\frac{1}{\delta + z} - Pe_m\right)\frac{dc}{dz} - \varphi^2c^p - \frac{Pe_m}{\delta + z}c = 0 \tag{5}$$

where δ denotes the geometry parameter, which is specified as the ratio of the inner membrane radius rin to its thickness L. In the limit where $\delta \gg 1$, the cylindrical model Eq. (5) results in the model equation for planar geometry, as given by Eq. (2).

Lemma 2. Let c represent a solution to the problem defined by Eq. (2) and (3) for Pem ≥ 0. Then,

$$0 \le c \le 1. \tag{6}$$

Proof. See Appendix in *Supporting Information file*.

To define a weak solution to Eq. (2) subject to the boundary conditions (3), we consider the space functions which are square-integrable over the spatial interval (0,1):

$$L^2(0,1) = \{v: (0,1) \rightarrow \mathbb{R}: \int_0^1 v^2(z)\,dz < \infty\},$$

This space is endowed with the L^2 norm defined as $\| v \|_0 = \left(\int_0^1 v^2(z)\,dz\right)^{1/2}$. Furthermore, we introduce the Sobolev space

$$H^1(0,1) = \{v: (0,1) \rightarrow \mathbb{R}: \frac{dv}{dz} \in L^2(0,1)\}$$

of functions in $L^2(0,1)$ whose weak derivatives are also in $L^2(0,1)$. The space $H^1(0,1)$ is equipped with the norm $\| v \|_1 = \left(\int_0^1 \left\{v^2(z) + \left(\frac{dv}{dz}\right)^2\right\} dz\right)^{1/2}$ and the semi-norm $|v|_1 = \left(\int_0^1 \left(\frac{dv}{dz}\right)^2 dz\right)^{1/2}$. Furthermore, we denote by $H^1_{D,0}(0,1)$ the test space of functions $v \in H^1(0,1)$ such that the Dirichlet condition $v(0) = 0$ is satisfied.

By introducing the new unknown u=1−c, the boundary value problem described by Eq. (2)-(3) can be reformulated as

$$-\frac{d^2u}{dz^2} + Pe_m\frac{du}{dz} = \varphi^2(1-u)^p \quad \text{in } (0,1), \tag{7}$$

subject to the boundary conditions

$$u(0) = 0 \quad \text{and} \quad \frac{du}{dz}(1) = 0. \tag{8}$$

The function $u \in H^1_{D,0}(0,1)$ is said to be a weak solution to Eq. (7)-(8) if u satisfies

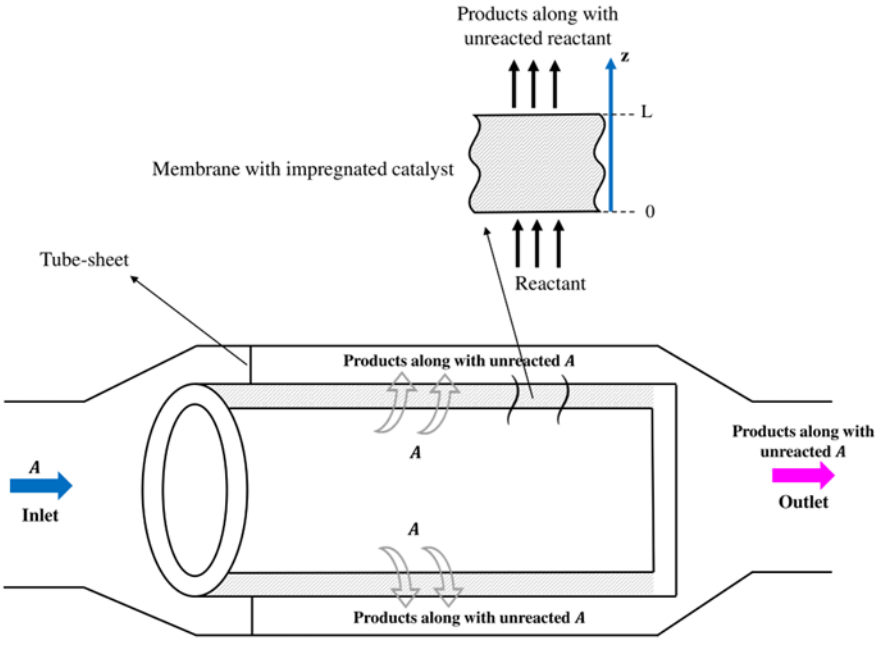

Fig. 1: Flow-through catalytic membrane reactor.

$$\int_0^1 \left(\frac{du}{dz}\frac{dv}{dz} + Pe_m \frac{du}{dz} v\right) dz = \varphi^2 \int_0^1 (1-u)^p v \, dz = 0 \quad \text{for all} \quad v \in H^1_{D,0}(0,1)\,. \tag{9}$$

The existence of the weak solution u will be shown by transforming the boundary value problem by (7)-(8) into the equivalent non-linear integral equation. Alternatively, the existence of the weak solution follows from the Browder-Minty Theorem (48) which requires advanced tools from functional analysis and will be omitted in this work. Let $G(z,y)$ denote the Green function associated with the differential operator $L[u] := -\frac{d^2u}{dz^2} + Pe_m \frac{du}{dz}$ subject to the boundary conditions by Eq. (8). Then,

$$G(z,y) = \begin{cases} \dfrac{1-e^{-Pe_m y}}{Pe_m}, & z \geq y\,, \\ \dfrac{e^{-Pe_m(y-z)}}{Pe_m} - \dfrac{e^{-Pe_m y}}{Pe_m}, & z \leq y\,, \end{cases} \tag{10}$$

and the boundary value problem by (7)-(8) turns into the Hammerstein integral equation

$$u(z) = \varphi^2 \int_0^1 G\,(z,y)(1-u(y))^p \, dy\,. \tag{11}$$

The existence of continuous solution u to Eq. (11) can be concluded from the Existence Theorem for Hammerstein Equations:

Theorem 3. *If $K(z,y)$ is continuous for $a \leq z, y \leq b$, and $f(y,w)$ is continuous and bounded for $a \leq y \leq b$ and all w, then the Hammerstein integral equation $u(z) = \int_a^b K\,(z,y) f(y,u(y))\, dy$ has a continuous solution $u(z)$.*

Proof. See Theorem 6.45 in (49).

Finally, we obtain;

Theorem 4. *The non-linear boundary value problem described by Eq. (2) and (3) possesses a unique weak solution for $Pe_m \geq 0$*

3. Dead-core solutions

Let $p \in [0,1)$. Then, the solution to the boundary value problem by Eq. (2)-(3) exhibits a dead zone if the Thiele modulus is sufficiently large. In the case of non-vanishing convection, *i.e.*, $Pe_m > 0$, finding analytically the critical Thiele modulus φ^*_{p,Pe_m} is not feasible. We denote the critical Thiele modulus by φ^*_{p,Pe_m} to emphasize that its value depends on a certain combination of the mass Peclet number Pe_m and fractional reaction exponent p. We will provide the closed-form expressions for the critical Thiele modulus only for two special cases. In the case of vanishing convection, *i.e.*, $Pe_m = 0$, the boundary value problem by Eq. (2)-(3) possesses the following non-classical solution

$$c(z) = \begin{cases} \left(\sqrt{\dfrac{\varphi^2(1-p)^2}{2(1+p)}}\,(z_{dz} - z)\right)^{\frac{2}{1-p}}, & 0 \leq z \leq z_{dz}\,, \\ 0\,, & z_{dz} \leq z \leq 1\,, \end{cases} \tag{12}$$

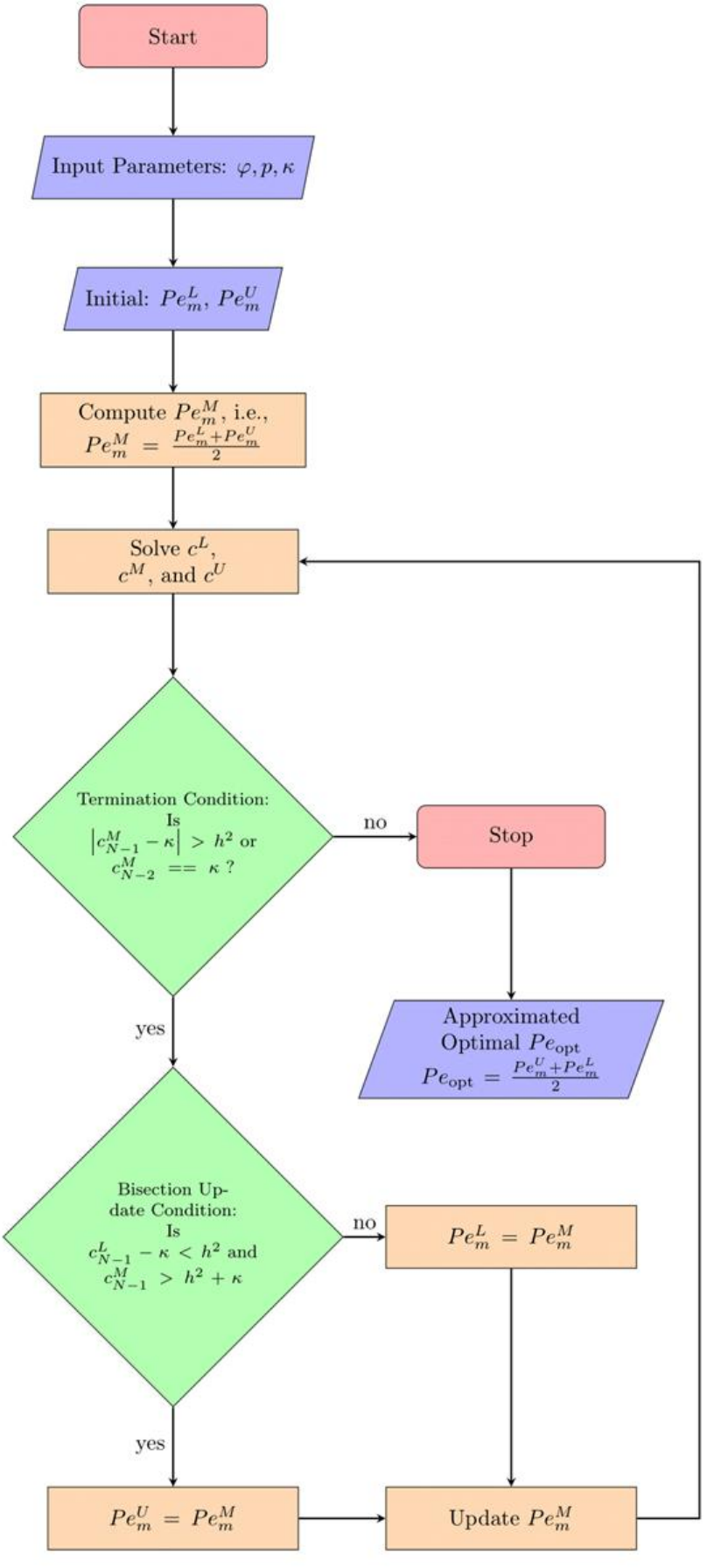

Fig. 2: Process flow diagram for bisection algorithm to determine optimal Pe_{opt}.

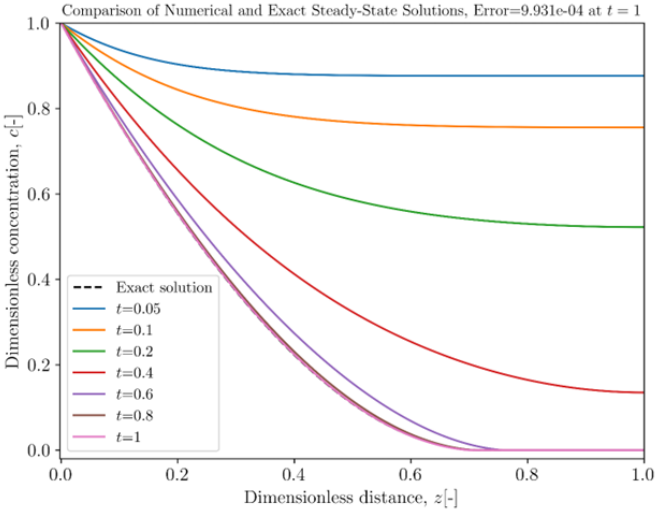

Fig. 3: Profiles of concentration $c(z,t)$ at various times for zero reaction exponent ($p = 0$) and $\varphi = 2.2$, $Pe_m = 1$.

if $\varphi > \varphi^*_{p,0}$ where

$$\varphi^*_{p,0} = \sqrt{\frac{2(1+p)}{(1-p)^2}} \tag{13}$$

denotes the critical Thiele modulus. Here,

$$z_{dz} = \sqrt{\frac{2(1+p)}{\varphi^2(1-p)^2}} = \frac{\varphi^*_{p,0}}{\varphi} \tag{14}$$

stands for the start position of the dead zone (27). If $\varphi = \varphi^*$, then the dead zone is trivial, *i.e.*, it is only one point $z = 1$, and the critical solution corresponding to the initiation of the dead zone reads as follows

$$c^*(z) = (1-z)^{\frac{2}{1-p}}. \tag{15}$$

Now, let us consider the case of non-vanishing convection ($Pe_m > 0$) and zero reaction exponent ($p = 0$). In this case, $c^0_+ = \text{sign}(c_+)$ where $sign$ is the signum function that determines the sign of its argument. Then, the two-point boundary value problem

$$\begin{gathered} \frac{d^2c}{dz^2} - Pe_m\frac{dc}{dz} - \varphi^2\text{sign}(c_+) = 0 \quad \text{in } (0,1), \\ c(0) = 1, \quad \frac{dc}{dz}(1) = 0 \end{gathered} \tag{16}$$

has for

$$\varphi^*_{0,Pe_m} = \frac{Pe_m}{\sqrt{Pe_m + e^{-Pe_m} - 1}} \tag{17}$$

the following critical solution

$$\begin{aligned} c^*(z) = \frac{(\varphi^*_{0,Pe_m})^2}{Pe_m^2}e^{Pe_m(z-1)} - \frac{(\varphi^*_{0,Pe_m})^2}{Pe_m}z + \\ 1 - \frac{(\varphi^*_{0,Pe_m})^2}{Pe_m^2}e^{-Pe_m} \end{aligned} \tag{18}$$

such that $c^*(z) > 0$ for $0 \le z < 1$ and $c^*(1) = 0$. It follows from the L'Hopital's rule that

$$\lim_{Pe_m\to 0^+}\varphi^*_{0,Pe_m} = \lim_{Pe_m\to 0^+}\frac{Pe_m}{\sqrt{Pe_m + e^{-Pe_m} - 1}} = \sqrt{2} \tag{19}$$

which coincides with $\varphi^*_{p,0}|_{p=0} = \sqrt{2}$ by Eq. (13). Furthermore, in the case of $p = 0$, the critical solution $c^*(z) = (1-z)^2$ by Eq. (15) can be recovered by passing in Eq. (18) to the limit as $Pe_m \to 0^+$, and using the Taylor expansion for $c^*(z)$ from Eq. (18) as follows

$$c^*(z) = (z-1)^2 + \frac{Pe_m}{3}((z-1)^2 + (z-1)^3) + \mathcal{O}(Pe_m^2).$$

If the Thiele modulus exceeds its critical value given by Eq. (17), then the solution to the two-point boundary value problems exhibits a dead-zone of length $1 - z_{dz}$. To determine the transition point z_{dz}, let us introduce the transformation $\xi = \frac{z}{z_{dz}} \in [0,1]$ for $z \in [0, z_{dz}]$, and set $\hat{c}(\xi) = c(\frac{z}{z_{dz}})$. Then, the two-point boundary value problem (16) can be transformed for $\varphi \ge \varphi^*_{0,Pe_m}$ as follows

$$\begin{gathered} -\frac{d^2\hat{c}}{d\xi^2} + z_{dz}Pe_m\frac{d\hat{c}}{d\xi} + z_{dz}^2\varphi^2 = 0 \quad \text{in } (0,1), \\ \hat{c}(0) = 1, \quad \frac{d\hat{c}}{d\xi}(1) = 0. \end{gathered} \tag{20}$$

Its solution is given by

$$\begin{aligned} \hat{c}(\xi) = \frac{\varphi^2}{Pe_m^2}e^{z_{dz}Pe_m(\xi-1)} - \frac{\varphi^2 z_{dz}}{Pe_m}\xi + 1 \\ - \frac{\varphi^2}{Pe_m^2}e^{-z_{dz}Pe_m}, \quad 0 \le \xi \le 1, \end{aligned} \tag{21}$$

where $\hat{c}|_{\xi=1} = 0$. Therefore, z_{dz} satisfies the following condition

$$\frac{\varphi^2}{Pe_m^2} - \frac{\varphi^2 z_{dz}}{Pe_m} + 1 - \frac{\varphi^2}{Pe_m^2}e^{-z_{dz}Pe_m} = 0, \tag{22}$$

from which we infer

$$z_{dz} = \frac{1}{Pe_m}\left[W\left(-e^{-\frac{Pe_m^2+\varphi^2}{\varphi^2}}\right) + \frac{Pe_m^2 + \varphi^2}{\varphi^2}\right], \tag{23}$$

Table 2: The maximum errors $e_i = \max_{j=1,\dots,N-1} |c(z_j) - c_j|$ between the exact solution $c(z_j)$ and numerical solution c_j at the interior spatial mesh points z_j, $j = 1, \dots, N-1$, and the orders of convergence for the boundary value problem by Eq. (2)-(3) with (a) $Pe_m = 1$, $p = 1$, $\varphi = 10$; (b) $Pe_m = 0$, $p = 0.5$, $\varphi = 10$; (c) $Pe_m = 1$, $p = 0$, $\varphi = 10$. The spatial mesh size on the refinement level i is given by $h_i = 2^{1-i}10^{-1}$.

level	(a)		(b)		(c)	
i	error e_i	order $\log_2\left(\frac{e_i}{e_{i+1}}\right)$	error e_i	order $\log_2\left(\frac{e_i}{e_{i+1}}\right)$	error e_i	order $\log_2\left(\frac{e_i}{e_{i+1}}\right)$
1	8.7413e−3		7.7098e−3		7.8425e−3	
2	1.3552e−3	2.68938	1.7049e−3	2.17702	1.6075e−3	2.28650
3	2.8932e−4	2.22771	4.0271e−4	2.08189	3.8349e−4	2.06757
4	6.9279e−5	2.06219	9.8946e−5	2.02501	9.5005e−5	2.01309
5	1.7130e−5	2.01587	2.4435e−5	2.01768	2.3665e−5	2.00525
6	4.2558e−6	2.00905	6.0902e−6	2.00440	5.9090e−6	2.00177

where W denotes the principal branch of the Lambert W function $W: [-1/e, +\infty) \to [-1, +\infty)$ which is defined as a solution $W(x) \geq -1$ to the equation $We^W = x$ for $x \in [-1/e, \infty)$. Note that if $Pe_m > 0$, then the transition point z_{dz} does not satisfy the relation $z_{dz} = \frac{\varphi^*_{0,Pe_m}}{\varphi}$ as it is the case when $Pe_m = 0$, cf. Eq. (14). Notice that we recover the value of the critical Thiele modulus φ^*_{0,Pe_m} from Eq. (17) by setting $z_{dz} = 1$ in Eq. (22).

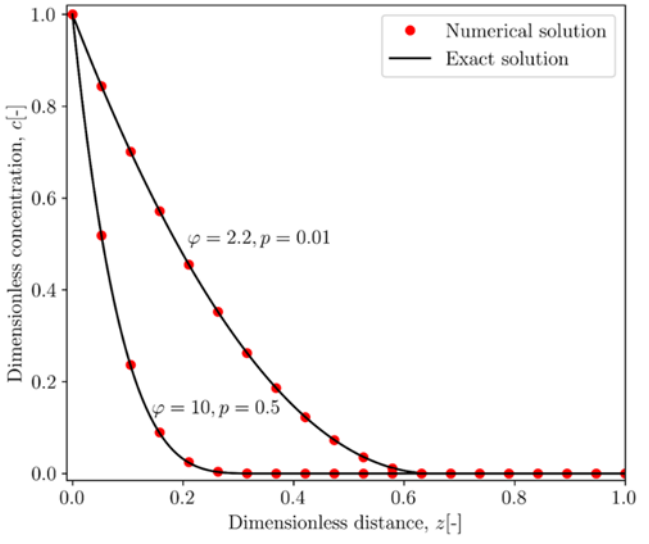

Fig. 4: Profiles of exact and numerical solutions with dead zones to boundary value problem by Eq. (25)-(26) for vanishing convection ($\mathrm{Pe_m} = 0$).

The dead-core solution to the problem with non-vanishing convection is given for $\varphi \geq \varphi^*_{0,Pe_m}$ as follows

$$c(z) = \begin{cases} \frac{\varphi^2}{Pe_m^2} e^{Pe_m(z-z_{dz})} - \frac{\varphi^2}{Pe_m} z + 1 - \frac{\varphi^2}{Pe_m^2} e^{-z_{dz}Pe_m}, & 0 \leq z \leq z_{dz}, \\ 0, & z_{dz} \leq z \leq 1, \end{cases} \quad (24)$$

where the transition point z_{dz} is defined by Eq. (23).

4. Time-marching method

The solution c(z) is approximated using a time-marching method. This approach involves considering the following transient equation:

$$\frac{\partial \tilde{c}}{\partial t} - \frac{\partial^2 \tilde{c}}{\partial z^2} + Pe_m \frac{\partial \tilde{c}}{\partial z} + \varphi^2 \tilde{c}^p = 0 \quad (25)$$

subject to the following boundary and the initial conditions

$$\tilde{c}(0,t) = 1\,, \quad \frac{\partial \tilde{c}}{\partial z}(1,t) = 0 \quad \text{for} \quad t > 0\,, \qquad \tilde{c}(z,0) = 1 \quad \text{for} \quad z \in (0,1)\,. \quad (26)$$

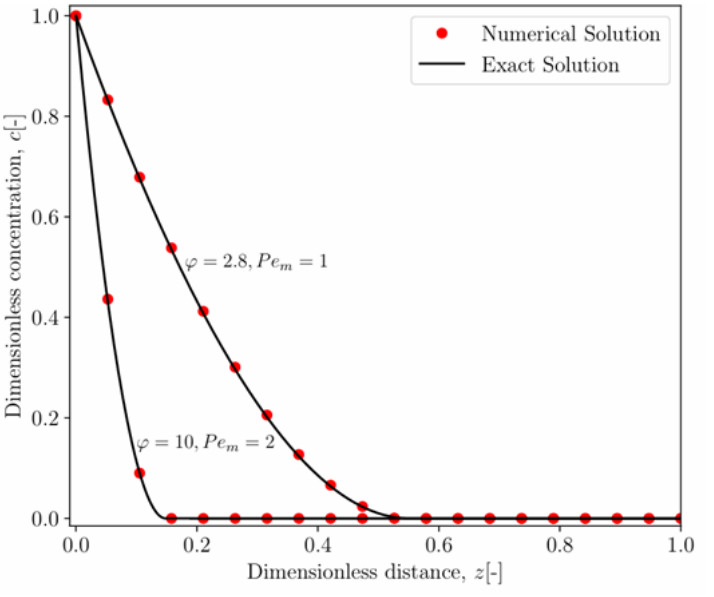

Fig. 5: Profiles of exact and numerical and solutions with dead zones to boundary value problem by Eq. (25)-(26) for non-vanishing convection ($Pe_m = 1{,}2$) and $p = 0$

Table 3: The absolute errors $e_i = \left|Pe_m - Pe_{\text{opt}}^{(i)}\right|$ between the exact optimal mass Peclet number Pe_m and approximate optimal mass Peclet number $Pe_{\text{opt}}^{(i)}$ computed on the spatial mesh level i, along with corresponding orders of convergence for the following cases: (a) $\varphi = 3$ and $Pe_m = 7.85462$; (b) $\varphi = 5$ and $Pe_m = 23.95644$; (c) $\varphi = 10$ and $Pe_m = 98.98979$. The spatial mesh size on the refinement level i is given by $h_i = 2^{1-i}10^{-1}$.

level	(a)		(b)		(c)	
i	error e_i	order $\log_2\left(\frac{e_i}{e_{i+1}}\right)$	error e_i	order $\log_2\left(\frac{e_i}{e_{i+1}}\right)$	error e_i	order $\log_2\left(\frac{e_i}{e_{i+1}}\right)$
1	1.1837e+0		2.8628e+0		1.0709e+1	
2	5.5826e−1	1.08425	1.3491e+0	1.08541	5.2398e+0	1.03118
3	2.7162e−1	1.03935	6.6551e−1	1.01947	2.5543e+0	1.03661
4	1.3264e−1	1.03406	3.2982e−1	1.01279	1.2725e+0	1.00522
5	6.5664e−2	1.01436	1.6350e−1	1.01240	6.3164e−1	1.01050
6	3.2799e−2	1.00145	8.1342e−2	1.00720	3.1578e−1	1.00018

The time-dependent solution $\tilde{c}(\cdot, t)$ to the boundary/initial value problem (25)-(26) converges exponentially fast with respect to the L^2-norm to the solution c of (2)-(3) as the time tends to infinity. Particularly, it holds true (46, Lemma 2)

$$\| \tilde{c}(\cdot, t) - c \|_0 \leq \| \tilde{c}(\cdot, 0) - c \|_0 \; e^{-2t}. \tag{27}$$

An analogous inequality can be shown for problems posed over multidimensional domains and with reaction terms that are monotonically increasing with respect to the concentration.

4.1 Modified Crank-Nicolson scheme

The Crank-Nicolson-based method(50) is used to obtain approximations to c̃(z_j,t_n) at certain spatial mesh points z_j, $j = 1, \ldots, N-1$, and discrete times t_n. The method is employed for the discretization of Eq. (25) and (26) with respect to time followed by finite difference approximation in space. The temporal derivative is discretized as $\frac{{c_j}^{n+1} - {c_j}^n}{\Delta t}$, while the first and second order spatial derivatives are discretized as $\frac{1}{2}\left(\frac{c_j^{n+1} - c_{j-1}^{n+1}}{h} + \frac{c_j^n - c_{j-1}^n}{h}\right)$ and $\frac{1}{2}\left(\frac{c_{j-1}^{n+1} - 2c_j^{n+1} + c_{j+1}^{n+1}}{h^2} + \frac{c_{j-1}^n - 2c_j^n + c_{j+1}^n}{h^2}\right)$, respectively. Furthermore, the reaction term $\tilde{c}^p$ is discretized as $\frac{1}{2}\left(\left(c_j^{n+1}\right)^p + \left(c_j^n\right)^p\right)$. Substituting the aforementioned discretized terms into Eq. (25) results in:

$$\begin{aligned} \frac{{c_j}^{n+1} - {c_j}^n}{\Delta t} = {} & \frac{1}{2h^2} c_{j+1}^{n+1} + \frac{1}{2}\left(\frac{-2}{h^2} - \frac{Pe_m}{h}\right) c_j^{n+1} + \frac{1}{2}\left(\frac{1}{h^2} + \frac{Pe_m}{h}\right) c_{j-1}^{n+1} \\ & + \frac{1}{2h^2} c_{j+1}^n + \frac{1}{2}\left(\frac{-2}{h^2} - \frac{Pe_m}{h}\right) c_j^n + \frac{1}{2}\left(\frac{1}{h^2} + \frac{Pe_m}{h}\right) c_{j-1}^n \\ & - \frac{1}{2}\varphi^2\left(\left(c_j^{n+1}\right)^p + \left(c_j^n\right)^p\right), \quad j = 1, \ldots, N-2. \end{aligned} \tag{28}$$

For $j = 1$, applying the boundary condition at the membrane inlet, we have $c_0^{n+1} = c_0^n = 1$. The Neumann boundary condition at the membrane outlet when $j = N-1$ can be discretized using second-order central difference approximation as $\frac{c_N^n - c_{N-2}^n}{2h} = \frac{c_N^{n+1} - c_{N-2}^{n+1}}{2h} = 0$.

Let $\mathbf{A} \in \mathbb{R}^{(N-1)\times(N-1)}$ be a square tridiagonal matrix defined as follows

$$\mathbf{A} = \begin{pmatrix} \alpha & \beta & & & 0 \\ \gamma & \alpha & \beta & & \\ & \ddots & \ddots & & \ddots \\ & & \gamma & \alpha & \beta \\ 0 & & & \gamma & \alpha + \beta \end{pmatrix},$$

where

$$\alpha = -\frac{2}{h^2} - \frac{Pe_m}{h}, \quad \beta = \frac{1}{h^2}, \quad \gamma = \frac{1}{h^2} + \frac{Pe_m}{h},$$

Table 4: Exact optimal mass Peclet number (Pe_m) for p=0, φ=5 and various values of κ.

κ	Exact mass Peclet number (Pe_m)
0.0	24.99991
0.2	31.24999
0.4	41.66667
0.6	62.49999
0.8	124.99999

Table 5: Approximate optimal mass Peclet number Pe_{opt} for various values of κ, reaction exponent p, and with $\varphi = 5$.

κ	Approximate optimal mass Peclet number Pe_{opt}			
	$p = 0.01$	$p = 0.2$	$p = 0.4$	$p = 0.6$
0.0	23.37638	17.34694	10.74215	3.12499
0.2	29.68597	25.92468	22.18628	18.69964
0.4	40.03906	36.84489	33.63037	30.56844
0.6	60.69946	57.86133	54.96216	52.15454
0.8	122.55859	119.99512	117.30957	114.74609

Then, the non-linear algebraic system by Eq. (28) can be written as

$$\frac{\mathbf{c}^{(n+1)}-\mathbf{c}^{(n)}}{\Delta t}=\frac{1}{2}\mathbf{A}\mathbf{c}^{(n+1)}+\frac{1}{2}\mathbf{A}\mathbf{c}^{(n)}-\frac{\varphi^2}{2}\left((\mathbf{c}^{(n+1)})^p+(\mathbf{c}^{(n)})^p\right)+\mathbf{f}$$

where

$$\mathbf{c}^{(n+1)}=[c_1^{(n+1)},\dots,c_{N-1}^{(n+1)}]^T,$$
$$\mathbf{c}^{(n)}=[c_1^{(n)},\dots,c_{N-1}^{(n)}]^T,$$
$$\mathbf{f}=[\frac{1}{h^2}+\frac{Pe_m}{h},0,\dots,0]^T.$$

For brevity, we define $\mathbf{c}^p := [(\max\{c_1,0\})^p,\dots,(\max\{c_{N-1},0\})^p]^T$ for $\mathbf{c}=[c_1,\dots,c_{N-1}]^T$. Then, the non-linear algebraic equation for the approximate dimensionless concentration $\mathbf{c}^{n+1}$ at each new time step is derived as

$$\mathbf{c}^{(n+1)}=\left(\mathbf{I}-\frac{1}{2}\Delta t\mathbf{A}\right)^{-1}\left\{\mathbf{c}^{(n)}+\frac{\Delta t}{2}\mathbf{A}\mathbf{c}^{(n)}-\frac{\varphi^2\Delta t}{2}\left((\mathbf{c}^{(n+1)})^p+(\mathbf{c}^{(n)})^p\right)+\Delta t\mathbf{f}\right\}. \tag{29}$$

The above algebraic system for the unknown vector $\mathbf{c}^{(n+1)}$ rep resents an equation of fixed-point type. We solved it numerically by employing N_{FPI} sweeps of the following fixed-point iteration:

$$\begin{aligned}
&\mathbf{c}^{(n+1),0}=\mathbf{c}^{(n)},\\
&\bar{\mathbf{c}}^{(n+1),\ell}=\left(\mathbf{I}-\frac{1}{2}\Delta t\mathbf{A}\right)^{-1}\left\{\mathbf{c}^{(n)}+\frac{\Delta t}{2}\mathbf{A}\mathbf{c}^{(n)}-\frac{\varphi^2\Delta t}{2}\left((\mathbf{c}^{(n+1),\ell-1})^p+(\mathbf{c}^{(n)})^p\right)+\Delta t\mathbf{f}\right\},\\
&\mathbf{c}^{(n+1),\ell}=\frac{1}{2}\max\{\bar{\mathbf{c}}^{(n+1),\ell},\mathbf{0}\}+\frac{1}{2}\max\{\mathbf{c}^{(n)},\mathbf{0}\},
\end{aligned} \tag{30}$$

where $\ell = 1,2,\dots,N_{\text{FPI}}$. For the approximate solution we finally set $\mathbf{c}^{(n+1)}=\mathbf{c}^{(n+1),N_{\text{FPI}}}$. In our computations, we employed $N_{\text{FPI}}\in\{2,3\}$. It is important to highlight that during each fixed-point iteration step ℓ we additionally performed an update based on the third equation in Eq. (30) to ensure that the approximate solution stays non-negative and converges toward the steady-state limit.

5. Bisection method for determining optimal Peclet number

5.1 Construction of upper non-dead-core solution Let us consider convection-diffusion-reaction equation with zero reaction exponent

$$\begin{aligned}
&\frac{d^2w}{dz^2}=Pe_m\frac{dw}{dz}+\varphi^2\text{sign}(w_+)\ \text{ in }\ (0,1),\\
&w(0)=1,\quad \frac{dw}{dz}(1)=0.
\end{aligned} \tag{31}$$

Since $\varphi^2c^p(z)\le\varphi^2\text{sign}(c_+)$ for $0\le c(z)\le 1$, $z\in(0,1)$, the solution to the problem by Eq. (31) which is given by Eq. (24) stays below the solution to the problem by Eq. (2)-(3). Our goal is to choose $Pe_m>0$ such that $w(1)=\kappa$ where $0\le\kappa<1$ is prescribed concentration value at the membrane outlet. Notice that $\kappa=0$ leads to the one-point dead-zone, *i.e.*, $z_{dz}=1$. Such a choice of $Pe_m>0$ ensures that $w>0$ in $(0,1)$. We have

$$w(z)=\frac{\varphi^2e^{-Pe_m(1-z)}}{Pe_m^2}-\frac{\varphi^2}{Pe_m}z+1-\frac{\varphi^2e^{-Pe_m}}{Pe_m^2}, \tag{32}$$

and consequently

$$\kappa=w(1)=\frac{\varphi^2}{Pe_m^2}-\frac{\varphi^2}{Pe_m}+1-\frac{\varphi^2e^{-Pe_m}}{Pe_m^2}=0, \tag{33}$$

from which we conclude that $Pe_m>0$ must satisfy the following transcendental equation

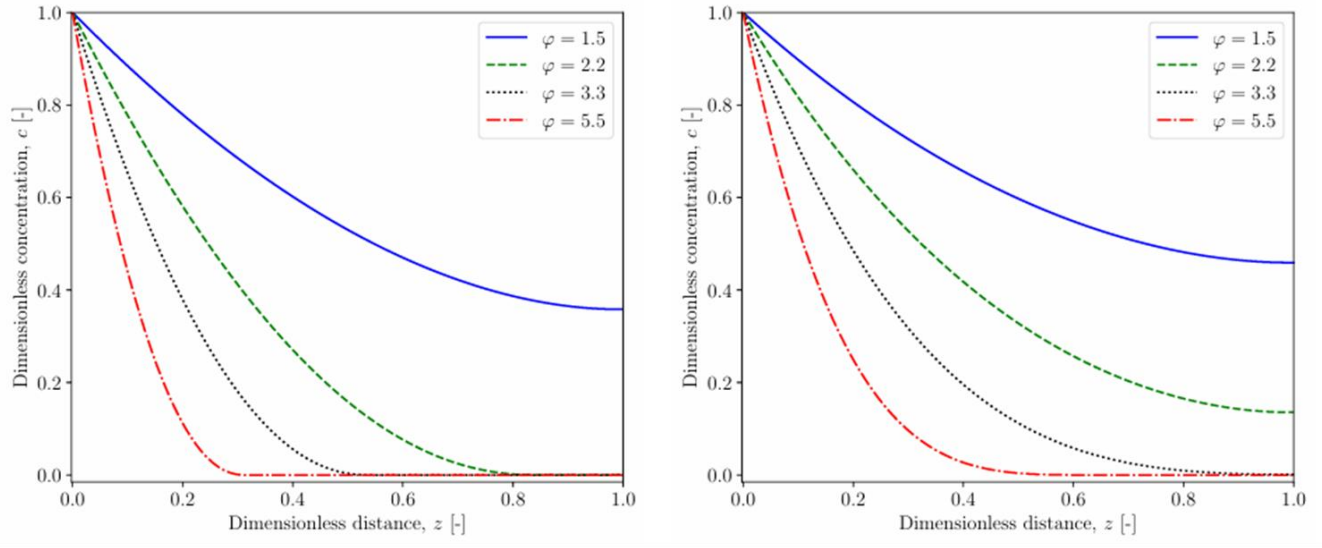

Fig. 6: Profiles of solutions with and without dead zones to boundary value problem by Eq. (25)-(26) for various values of Thiele modulus, φ, at (a) $Pe_m = 1, p = 0.1$ (b) $Pe_m = 1, p = 0.5$.

$$\frac{1-\kappa}{\varphi^2} = \frac{e^{-Pe_m}}{Pe_m^2} + \frac{1}{Pe_m} - \frac{1}{Pe_m^2}. \tag{34}$$

Let us denote the right side of Eq. (34) by $F(Pe_m)$, and notice that the transcendental equation

$$F(Pe_m) = \frac{1-\kappa}{\varphi^2} \tag{35}$$

does not possess a closed-form solution. The following lemma shows that the function $F(Pe_m)$ is monotonically decreasing on $(0, \infty)$.

Lemma 5. *The function* $F: (0, \infty) \to \mathbb{R}$ *with*

$$F(Pe_m) = \frac{e^{-Pe_m}}{Pe_m^2} + \frac{1}{Pe_m} - \frac{1}{Pe_m^2}$$

is positive and monotonically decreasing.

Proof. See Appendix in *Supporting Information file*.

To find an upper bound for solution $Pe_m > 0$ to Eq. (35), let us introduce the function $G: (0, \infty) \to \mathbb{R}$ with

$$G(Pe_m) = \frac{1 - e^{-\frac{1}{2}Pe_m}}{Pe_m}. \tag{36}$$

In the next lemma we show that $F(Pe_m) \leq G(Pe_m)$ for all $Pe_m > 0$.

Lemma 6. *The inequality*

$$\frac{e^{-Pe_m}}{Pe_m^2} + \frac{1}{Pe_m} - \frac{1}{Pe_m^2} \leq \frac{1 - e^{-\frac{1}{2}Pe_m}}{Pe_m} \tag{37}$$

is satisfied for all $Pe_m > 0$.

Proof. See Appendix in *Supporting Information file.*

In the next lemma, the solution to the nonlinear equation $G(Pe_m) = \frac{1-\kappa}{\varphi^2}$ in expressed in terms of the Lambert W function.

Lemma 7. *The nonlinear equation*

$$\frac{1 - e^{-\frac{1}{2}Pe_m}}{Pe_m} = \frac{1-\kappa}{\varphi^2} \tag{38}$$

has a solution given by

$$Pe_m = 2W\left(-\frac{1}{2}\frac{\varphi^2}{1-\kappa}e^{-\frac{1}{2}\frac{\varphi^2}{1-\kappa}}\right) + \frac{\varphi^2}{1-\kappa}. \tag{39}$$

Proof. See Appendix in *Supporting Information file*.

5.2 Bisection algorithm

Given the Thiele modulus $\varphi > 0$ and reaction exponent $p > 0$, consider the diffusion-reaction problem ($Pe_m = 0$) whose solution exhibits a dead zone. Then, for a prescribed outlet concentration $0 \leq \kappa < 1$, we will find the Peclet number $Pe_m > 0$ such that the corresponding convection-diffusion-reaction equation

$$\frac{d^2c}{dx^2} - Pe_m\frac{dc}{dx} - \varphi^2 c^p = 0\,, \quad c(0) = 1,\ \frac{dc}{dx}(1) = 0$$

satisfies $c(1) = \kappa$. This can be achieved through a numerical approach employing a modified Crank-Nicolson scheme and a bisection method. Let us denote by $\mathbf{c} \in \mathbb{R}^N$ with

$$\mathbf{c} = [c_0, c_1, c_2, \ldots, c_{N-2}, c_{N-1}]^T \quad \text{with } c_0 = 1$$

the nodal vector for the finite difference approximation is determined by Eq. (30), where $N \in \mathbb{N}$ represents the number

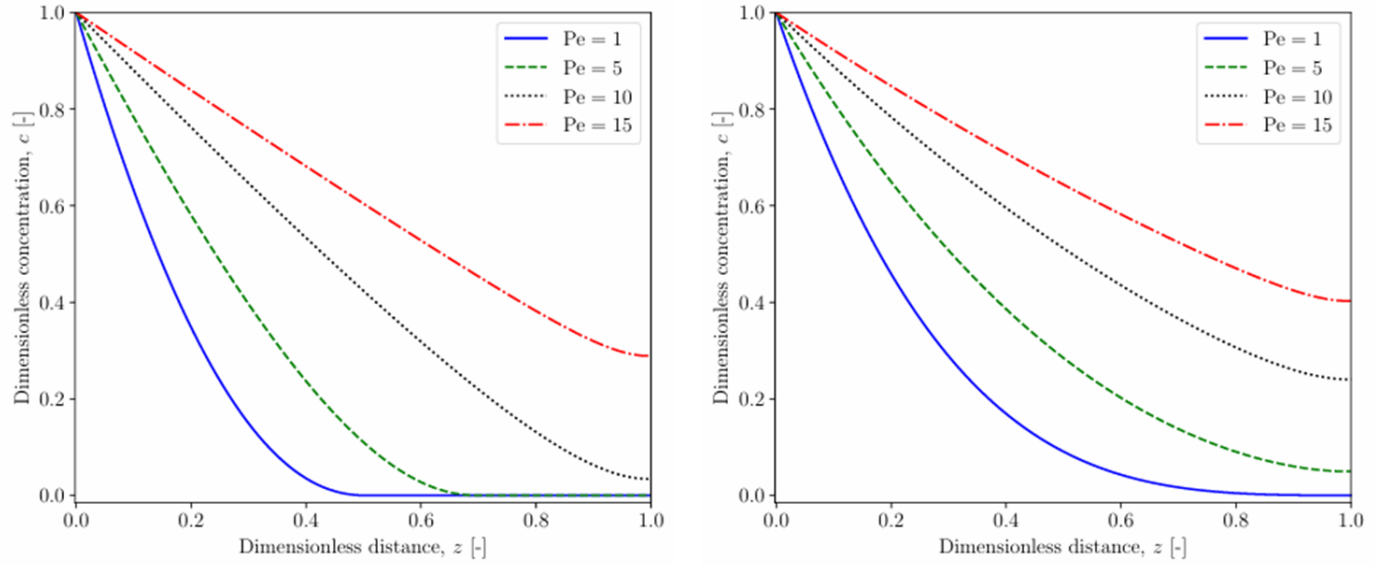

Fig. 7: Profiles of solutions with and without dead zones to boundary value problem by Eq. (25)-(26) for various values of mass Peclet number, Pe_m, at (a) $\varphi = 3.5$, $p = 0.1$ (b) $\varphi = 3.5$, $p = 0.5$.

of spatial grid points. The nodal solution is obtained through the application of the modified Crank-Nicolson scheme with a sufficiently large number of time steps.

A Python code is utilized to numerically solve the resulting sequence of nonlinear convection-diffusion-reaction equations, see Fig. 2 We obtain three different numerical solutions, denoted as $\mathbf{c}^L$, $\mathbf{c}^M$, and $\mathbf{c}^U$, corresponding to three different Peclet numbers Pe_m^L, Pe_m^M, and Pe_m^U, respectively, while keeping the parameters φ and p fixed. To solve the nonlinear convection-diffusion-reaction equation, the first step requires the specification of three parameters: φ, p, and κ, along with the number of grid points N. The mass Peclet number Pe_m is determined iteratively using the bisection algorithm, where in each bisection step, the following condition is verified

$$|\mathbf{c}_{N-1}^M - \kappa| > h^2 \quad \text{or} \quad \mathbf{c}_{N-2}^M = \kappa\,. \tag{40}$$

Here, $h = 1/(N-1)$ denotes the mesh size. The first iteration step in the bisection algorithm is initiated with

$$Pe_m^U = 2W\left(-\frac{1}{2}\frac{\varphi^2}{1-\kappa}e^{-\frac{1}{2}\frac{\varphi^2}{1-\kappa}}\right) + \frac{\varphi^2}{1-\kappa} \quad \text{and} \quad Pe_m^L = 0\,. \tag{41}$$

Then, we set

$$Pe_m^M = \frac{Pe_m^L + Pe_m^U}{2}.$$

If the main conditions by Eq. (40) holds and $\mathbf{c}_{N-1}^L - \kappa < h^2$ and $\mathbf{c}_{N-1}^M > h^2 + \kappa$, then the following update is perfomed $Pe_m^U = Pe_m^M$. Otherwise, $Pe_m^L = Pe_m^M$. The Python program continues to compute Pe_m^L, Pe_m^M, Pe_m^U iteratively by satisfying the conditions by Eq. (40) until the iteration is terminated and the approximate optimal Peclet number Pe_{opt} is set as the average of Pe_m^L and Pe_m^U from the last iteration.

6. Numerical results and discussion

6.1 Numerical validation of time marching scheme

To validate the proposed time-marching method for solving numerically the boundary value problem by Eq. (25)-(26), we consider various convection and reaction exponent scenarios. Fig. 3 presents transient solution for various times, along with the exact steady-state dead-core solution for $\varphi = 2.2$, $Pe_m = 1$, and $p = 0$.

The numerical solution converges exponentially fast to the exact steady-state solution

$$c(z) = \frac{\varphi^2}{Pe_m^2}e^{Pe_m z} - \frac{\varphi^2}{Pe_m}z + 1 - \frac{\varphi^2}{Pe_m^2} \tag{42}$$

for $\varphi < \varphi_{0,Pe_m}^* = \frac{Pe_m}{\sqrt{Pe_m + e^{-Pe_m} - 1}}$ as the time increases. This convergence is motivated by Eq. (27) since $c_j^n \approx \tilde{c}(z_j, t^n)$.

Fig. 4 presents a comparison between the approximate and exact solutions for the scenarios with vanishing convection ($Pe_m = 0$). First, the parameters were set to $\varphi = 2.2$ and $p = 0.01$. Then, the computation was repeated for $\varphi = 10$ and $p = 0.5$. The numerical solutions obtained using the spatial mesh with $N = 20$ nodes demonstrate high accuracy when compared to the exact solutions. The exact steady-state solution with dead zone is given by Eq. (12).

Table 2(a) presents the orders of convergence for the spatial errors in the case with non-vanishing convection and non-zero reaction exponent ($\varphi = 10$, $p = 1$ and $Pe_m = 1$).

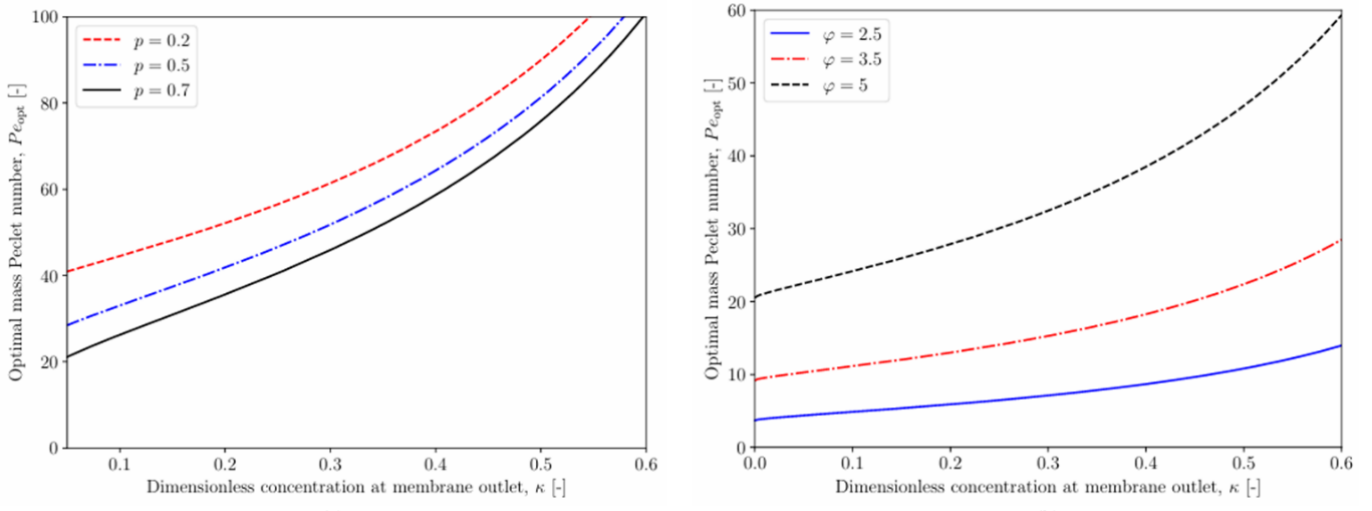

Fig. 8: Effect of κ on optimal mass Peclet number Pe_{opt} for (a) varying p at $\varphi = 7$, (b) varying φ at $p = 0.1$.

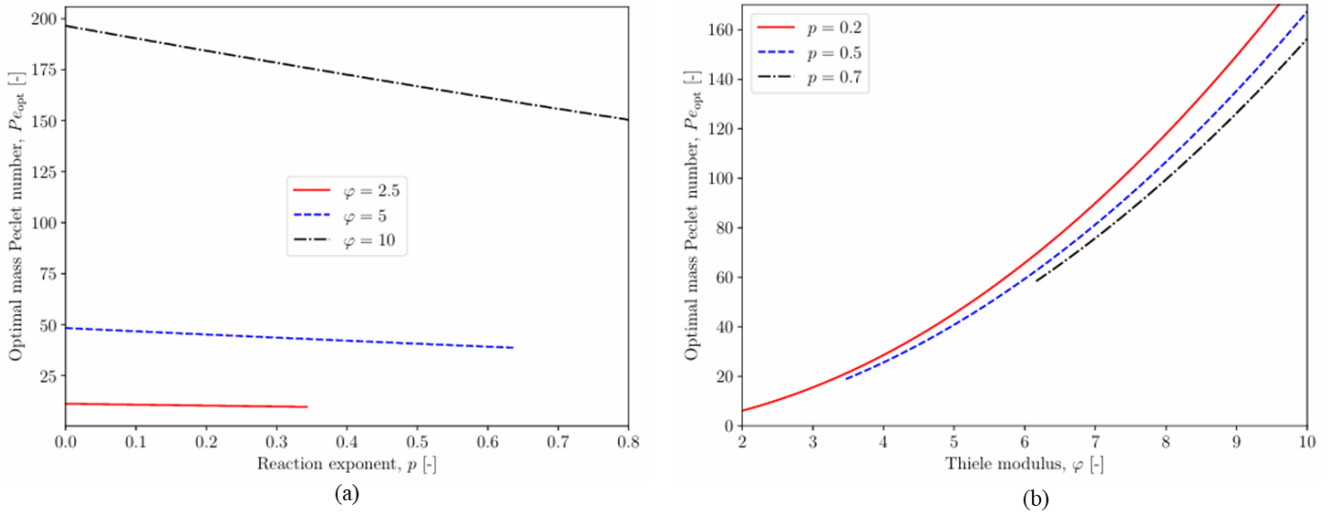

Fig. 9: Variation of the optimal mass Peclet number Pe_{opt} with respect to (a) the reaction exponent p, and (b) Thiele modulus φ for fixed value of $\kappa = 0.5$.

Table 2(b) shows the orders of convergence for the spatial errors for the scenario with vanishing convection and non-zero reaction exponent ($\varphi = 10$, $p = 0.5$ and $Pe_m = 0$). Table 2(c) provides the orders of convergence for the spatial errors in the case with non-vanishing convection and zero reaction exponent ($\varphi = 10$, $p = 0$ and $Pe_m = 1$). The numerical results in Table 2 demonstrate that the proposed time-marching scheme is second-order in space for both dead-core and non-dead-core solutions, as well as for cases with vanishing and non-vanishing convection. In all numerical tests, the temporal step was selected to be sufficiently small to minimize temporal discretization errors and ensure that the overall numerical error is dominated by spatial discretization errors.

In Fig. 5, the exact and numerical solutions to the dead-core problem are illustrated, as defined by Eq. (2)-(3) for non-vanishing convection ($Pe_m = 1, 2$) and zero reaction exponent. The numerical approximations align closely with the exact dead-core solutions provided by Eq. (24). These numerical tests demonstrate that the modified Crank-Nicolson scheme effectively handles problems involving non-vanishing convection and solutions with large dead zones.

6.2 Numerical validation of bisection algorithm for computing optimal Pe_m

Table 3 presents the orders of convergence for the absolute errors between the exact optimal Pe_m listed in Table 4 and the optimal mass Peclet number $Pe_{\text{opt}}^{(i)}$ computed using the bisection method designed in Section 5.2 for $\kappa = 0$. The absolute error on the spatial mesh with $h_i = 2^{1-i}10^{-1}$ was calculated as $e_i = \left|Pe_m - Pe_{\text{opt}}^{(i)}\right|$. The numerical tests were conducted for the case of zero reaction exponent ($p = 0$), various Thiele moduli ($\varphi = 3; 5; 10$), and $\kappa = 0$. We notice

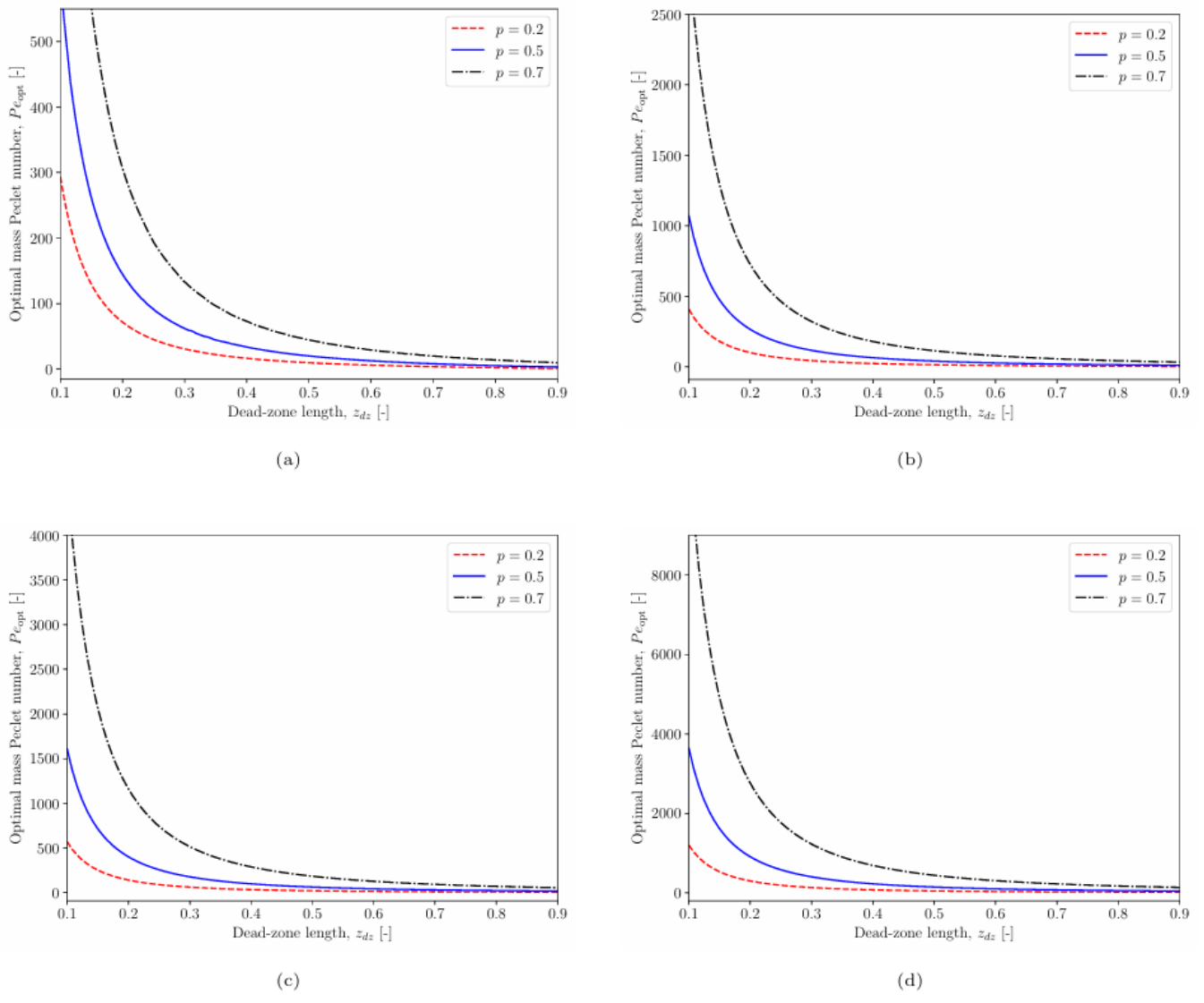

Fig. 10: Effect of dead-zone length z_{dz} on Pe_{opt} for various reaction exponent p at (a) $\kappa = 0$, (b) $\kappa = 0.2$, (c) $\kappa = 0.4$, and (d) $\kappa = 0.7$.

that the convergence of $Pe_{\text{opt}}^{(i)}$ towards Pe_m is of first order with respect to the spatial mesh size.

It is a well known fact that the speed of convergence of the bisection iteration is linear, and it holds the following a priori error estimate

$$|Pe_{\text{opt}}^{(k)} - Pe_m| \leq \frac{1}{2^k}|Pe_m^U - Pe_m^L|,$$

where $Pe_{\text{opt}}^{(k)}$ denotes the approximation in the k-th iteration step, Pe_m^U and Pe_m^L are the start values by Eq. (41). Therefore, the approximation error in the k-th bisection step is given by

$$|Pe_{\text{opt}}^{(k)} - Pe_m| \leq \frac{1}{2^k}\left\{2W\left(-\frac{1}{2}\frac{\varphi^2}{1-\kappa}e^{-\frac{1}{2}\frac{\varphi^2}{1-\kappa}}\right) + \frac{\varphi^2}{1-\kappa}\right\}.$$

In Table 5, the approximate optimal mass Peclet numbers Pe_{opt} are listed for various values of κ and reaction exponent p. The approximations were obtained on the fine spatial mesh with $h = 10^{-2}$, and using $\varphi = 5$.

6.3 Simulation results

6.3.1 Effect of Thiele modulus and Peclet number on concentration distribution

Fig. 6 (a) and (b) shows the dead-core and non-dead core solution profiles for the problem by Eq. (2)-(3) for various values of the Thiele modulus φ, and at the fixed Peclet number $Pe_m = 1$, and reaction exponents (a) $p = 0.1$ and (b) $p = 0.5$.

The concentration profiles exhibit a monotonic decrease with increasing Thiele modulus, which eventually leads to the formation of dead zones when the Thiele modulus exceeds its critical value. The opposite trend is observed in Fig. 7 (a) and (b), which show the solution profiles with and without dead zones across various mass Peclet numbers, with the Thiele modulus fixed at $\varphi = 3.5$. The profiles correspond to reaction exponents of (a) $p = 0.1$ and (b) $p = 0.5$.

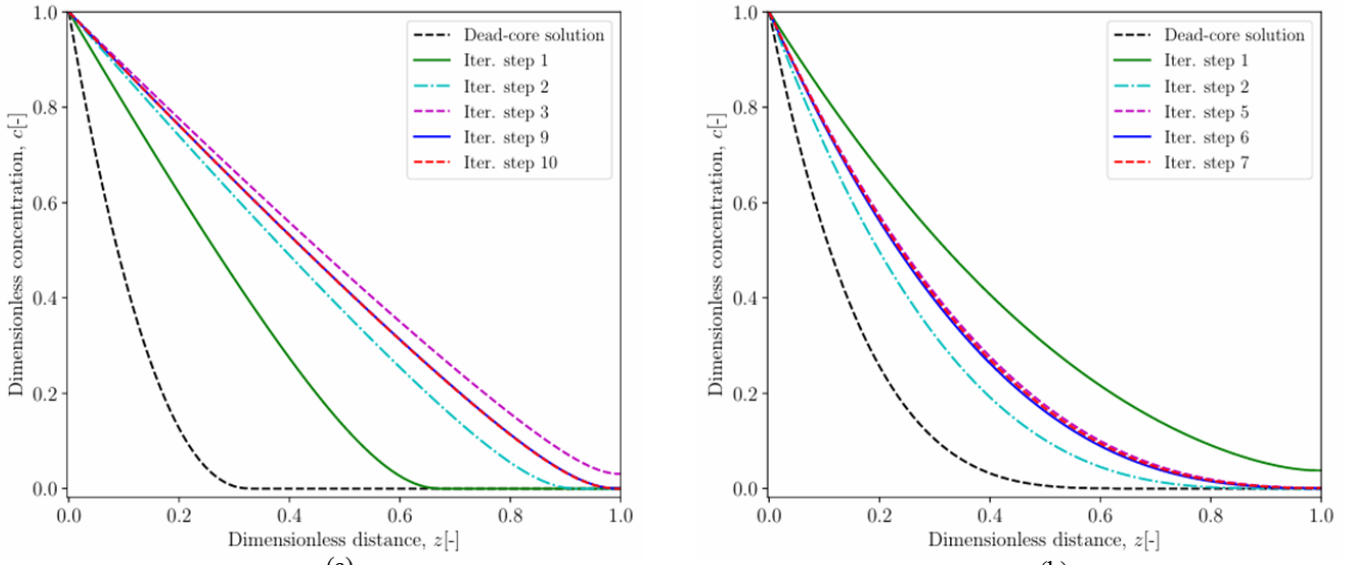

Fig. 11: Convergence of bisection iteration for $\varphi = 5$ and $\kappa = 0$ at (a) $p = 0.1$, (b) $p = 0.5$.

As the Peclet number increases, the concentration profiles exhibit a monotonic increase, leading to the suppression of dead zones when the Peclet number exceeds the critical value defined by Eq. (17). The time-marching scheme proves to be well-suited for handling cases with large dead-zones.

6.3.2 Effect of κ on optimal Peclet number Pe_{opt}

Fig. 8(a) illustrates the impact of dimensionless concentration at the membrane outlet, κ, on the optimal mass Peclet number, Pe_{opt}, for various values of the reaction exponent, p. As κ increases, Pe_{opt} also increases for all values of p, indicating that higher outlet concentrations require greater convective transport relative to diffusion to maintain optimal reaction efficiency. Notably, when $p = 0.2$, the required Pe_{opt} is higher compared to cases with fractional exponents, $p = 0.5$ and $p = 0.7$. This indicates that the case with reaction exponent, $p = 0.2$, requires more convective transport to achieve the same outlet concentration, likely due to its lower inherent reaction rate. In contrast, reactions with higher reaction exponents *i.e.*, $p = 0.5$ and $p = 0.7$ exhibit enhanced rates, reducing the need for convective transport and allowing lower mass Peclet numbers to reach similar outlet concentrations. This analysis highlights the importance of selecting appropriate mass Peclet numbers based on the reaction exponent and desired outlet concentration. In Fig. 8(b), the effect of κ on Pe_{opt} is shown for different values of Thiele modulus, φ. As φ increases, the required Pe_{opt} for a given κ also increases, indicating that convection-diffusion-reaction processes with a higher Thiele modulus require more convective transport to counter diffusion limitations and prevent dead core formation.

At higher φ values, there is an increased tendency for dead core regions to form, where the chemical reaction effectively ceases due to reactant depletion. To avoid this dead core, higher Pe_{opt} values are necessary, reflecting the increased mass transfer demands at high reaction rates. In contrast, lower φ values, such as $\varphi = 2.5$, exhibit only a slight increase in Pe_{opt} at higher κ values, indicating reduced dependency on convective transport at lower reaction rates.

6.3.3 Effect of p and φ on optimal Peclet number Pe_{opt}

Fig. 9(a) illustrates the effect of the reaction exponent p (where $|p| < 1$) on the optimal mass Peclet number, Pe_{opt}, for various values of the Thiele modulus, φ. As p increases, Pe_{opt} decreases, indicating that higher reaction exponents reduce the requirement for convective mass transport to achieve optimal reaction efficiency. This trend is especially pronounced at higher values of φ, with $\varphi = 10$ showing a substantial decrease in Pe_{opt} as p increases, suggesting greater adaptability to changes in reaction kinetics. At lower values of φ, such as $\varphi = 2.5$, the trend is nearly flat, indicating that Pe_{opt} remains relatively constant as p changes. For $\varphi = 5$, a slight decrease in Pe_{opt} is observed with increasing p, though this change is less pronounced than for $\varphi = 10$. These results suggest that higher values of φ lead to a greater sensitivity of Pe_{opt} to changes in p, thereby allowing a broader range of reaction kinetics to be accommodated effectively. Additionally, at higher φ values, there is a tendency for dead zones to form, which necessitates an increase in Pe_{opt} to sustain effective reaction performance and avoid dead zones within the membrane. This investigation underscores the significance of precisely balancing Pe_{opt} and φ in reactor design to attain optimal performance and mitigate the dead core formation,

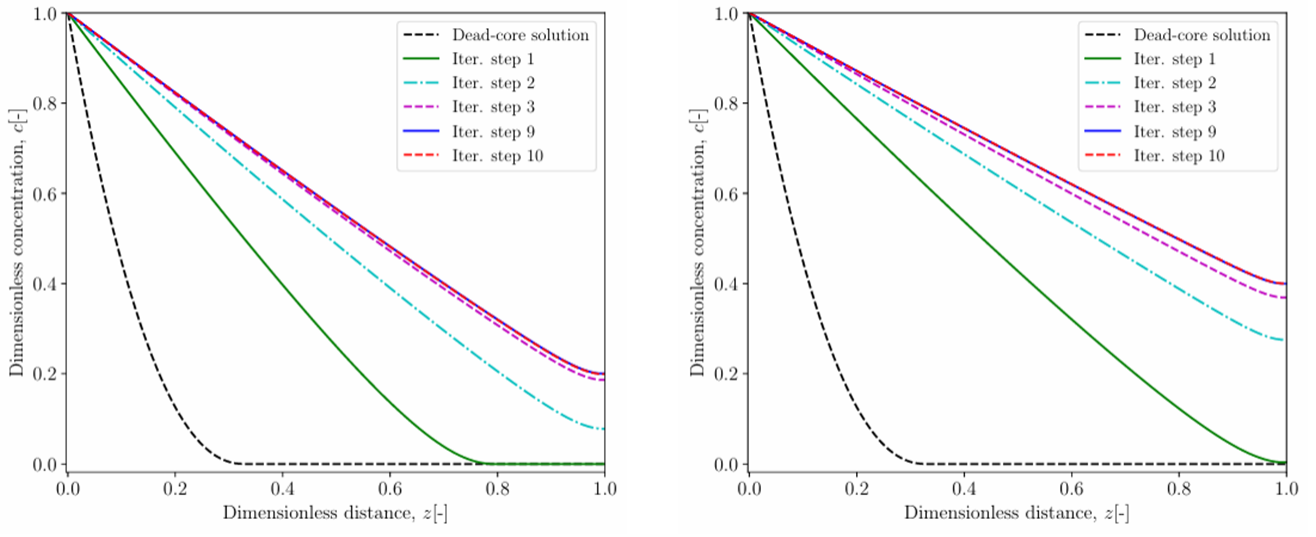

(a) (b)

Fig. 12: Convergence of bisection iteration with $\varphi = 5$ and $p = 0.1$ at (a) $\kappa = 0.2$ and (b) $\kappa = 0.4$.

particularly under conditions of varying reaction rates.

The impact of the Thiele modulus φ on the optimal mass Peclet number Pe_{opt} for varying reaction exponents p is shown in Fig 9(b). As φ increases, Pe_{opt} also increases, indicating that higher values of φ correspond to larger Pe_{opt} values. This trend is more pronounced for smaller reaction exponents, as indicated by the steeper curve for $p = 0.2$ in contrast to $p = 0.3$ and $p = 0.7$. The findings indicate that when p values increase, Pe_{opt} exhibits less sensitivity to variations in φ. This behavior aligns with the observations in Fig. 9(a), where higher p values similarly reduced the need for adjustments in convective transport.

6.3.4 Effect of dead-zone length z_{dz} on optimal Peclet number Pe_{opt}

Fig 10 (a), (b), (c), and (d) illustrate the effect of dead-zone length z_{dz} on the optimal mass Peclet number Pe_{opt} for various reaction exponents p and different values of dimensionless concentration κ, set at 0, 0.2, 0.4, and 0.7, respectively. In each of these figures, it is evident that as dead-zone length z_{dz} increases, Pe_{opt} decreases, with a more pronounced effect at shorter dead-zone lengths. The influence of the reaction exponent p suggests that higher p values lead to greater initial Pe_{opt} values, followed by a pronounced decline as z_{dz} increases. This trend indicates that higher reaction rates (larger p) require enhanced convective mass transport when the dead-zone length is small; however, this requirement diminishes as the dead-zone length grows. As shown in the figures, increasing dimensionless concentration κ has a clear impact.

As κ increases from 0 in Fig. 10(a) to 0.2 in Fig. 10(b), 0.4 in Fig. 10(c) and 0.7 in Fig. 10(d), the initial values of Pe_{opt} exhibit a substantial increase, particularly for elevated p values. This pattern suggests that higher κ requires a greater mass Peclet number to maintain optimal performance.

6.3.5 Convergence of bisection iteration for finding Pe_{opt}

Fig. 11 and 12 illustrate the convergence behavior of the bisection algorithm for various parameter settings. In all scenarios, the algorithm efficiently converges to the desired concentration profile, achieving the target outlet concentration κ within approximately 10 iterations.

The effect of reaction exponent on the convergence of the bisection algorithm is demonstrated for $\kappa = 0.4$ and $\varphi = 5$ in Fig. 13. In all cases, the bisection algorithm exhibits rapid convergence, achieving the prescribed outlet concentration κ within approximately 10 iteration steps.

Table 6: Values of dimensionless prescribed concentration at membrane outlet κ and corresponding approximations $c_1 \approx c(1)$, errors, and approximate optimal mass Peclet numbers Pe_{opt}, with parameters set as $\varphi = 3.5$, $p = 0.5$, and mesh size $h = 10^{-2}$.

κ	c_1	error	Pe_{opt}
0	2.70341e-5	2.70341e-5	0.76393
0.2	0.20005	4.52749e-5	8.96043
0.4	0.39996	4.25703e-5	14.90322
0.6	0.60004	4.01527e-5	25.55572
0.8	0.80009	9.31632e-5	56.28540

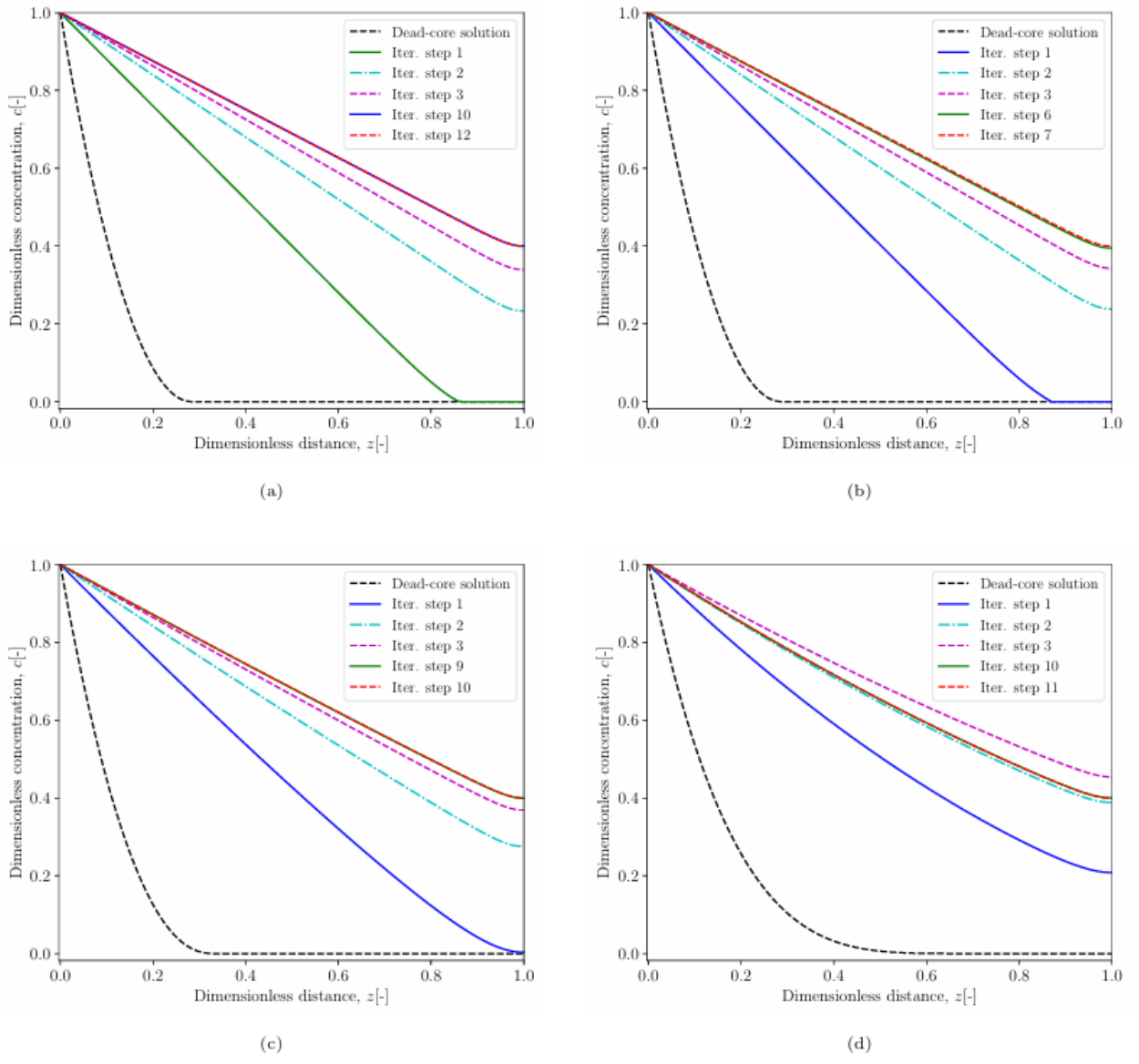

Fig. 13: Convergence of bisection iteration with $\varphi = 5$ and $\kappa = 0.4$, at (a) $p = 0$, (b) $p = 0.01$, (c) $p = 0.1$, and (d) $p = 0.5$.

Table 6 summarizes the values of dimensionless prescribed concentrations at membrane outlet κ, the corresponding approximations $c_1 \approx c(1)$, associated error, and the approximate optimal mass Peclet number Pe_{opt} under the conditions $\varphi = 3.5$, $p = 0.5$, and mesh size $h = 10^{-2}$. The values presented in the table underscore the accuracy of the approximation c_1 at the membrane outlet, along with its correlation to the optimal Peclet number, thereby offering validation of the model's predictions.

7. Conclusion

We proposed a simple yet efficient algorithm to suppress dead-zone formation in catalytic reactor mem- branes with a single reaction. The model describing the reactant concentration inside the catalytic membrane is governed by a nonlinear convection-diffusion-reaction equation

We showed that the formation of dead zone within the catalytic membrane can be suppressed by introducing with reaction term of power-law type.

The reaction kinetics with fractional reaction exponent can result in the formation of dead zones, regions within the catalytic membrane where the reaction ceases due to insufficient reactant supply through diffusion, leading to inefficient use of expensive catalyst. We developed an appropriate time-marching scheme since the class of dead-core problems requires special iterative approaches due to the non-differentiability of the reaction term at the vanishing concentration. We rigorously proved the existence and uniqueness of solutions to the two-point boundary value problems for nonlinear convection-diffusion-reaction equations and motivated the convergence of the time-marching scheme. We derived analytically the critical Thiele modulus for problems with non-vanishing convection and zero reaction exponent. additional convection characterized by the Peclet number. The proposed bisection algorithm for suppressing dead-

zone formation can be used to compute the optimal Peclet number required to achieve a desired outlet concentration. The presented theoretical findings are corroborated by numerical simulations conducted for scenarios with various model and process parameters. This work has significant implications for reactor design, offering potential improvements in efficiency and cost-effectiveness. Future research will extend the proposed bisection algorithm to non-isothermal catalytic membrane reactors to address dead-zone formation in more complex scenarios.

Acknowledgments
This research was funded in part by grant 20122022CRP1612 from Nazarbayev University, and Ulam NAWA grant BPN/ULM/2022/1/00164/DEC/1.

Conflict of Interest
There are no conflicts to declare.

Supporting Information
Applicable.

CRediT Statement
Piotr Skrzypacz: initiated and supervised the project. **Qaiser Abbas:** implemented the proposed bisection algorithm in Python, conducted numerical tests and simulations, and wrote and reviewed the manuscript. **Sławomir Szafert:** verified the modeling and simulation scenarios. **Vsevolod Andreev:** verified the analysis and simulation results. **Askar Amirali:** conducted analysis for the bisection algorithm. **Boris Golman:** reviewed the manuscript and verified the derived algorithm and formulas. The manuscript was written with contributions from all authors, who discussed the results and approved the final version.

References
[1] T. Westermann, T. Melin, Flow-through catalytic membrane reactors: principles and applications, *Chemical Engineering and Processing: Process Intensification*, 2009, **48**, 17-28, doi: 10.1016/j.cep.2008.07.001.
[2] A. Schmidt, R. Haidar, R. Schomäcker, Selectivity of partial hydrogenation reactions performed in a pore-through-flow catalytic membrane reactor, *Catalysis Today*, 2005, **104**, 305-312, doi: 10.1016/j.cattod.2005.03.073.
[3] M. M. Yousef Motamedhashemi, F. Egolfopoulos, T. Tsotsis, Application of a flow-through catalytic membrane reactor (FTCMR) for the destruction of a chemical warfare simulant, *Journal of Membrane Science*, 2011, **376**, 119-131, doi: 10.1016/j.memsci.2011.04.013.
[4] F. Gallucci, E. Fernandez, P. Corengia, M. van Sint Annaland, Recent advances on membranes and membrane reactors for hydrogen production, *Chemical Engineering Science*, 2013, **92**, 40-66, doi: 10.1016/j.ces.2013.01.008.
[5] J. Caro, K. J. Caspary, C. Hamel, B. Hoting, P. Kölsch, B. Langanke, K. Nassauer, T. Schiestel, A. Schmidt, R. Schomäcker, A. Seidel-Morgenstern, E. Tsotsas, I. Voigt, H. Wang, R. Warsitz, S. Werth, A. Wolf, Catalytic membrane reactors for partial oxidation using perovskite hollow fiber membranes and for partial hydrogenation using a catalytic membrane contactor, *Industrial & Engineering Chemistry Research*, 2007, **46**, 2286-2294, doi: 10.1021/ie0609620.
[6] R. Dittmeyer, V. Höllein, K. Daub, Membrane reactors for hydrogenation and dehydrogenation processes based on supported palladium, *Journal of Molecular Catalysis A: Chemical*, 2001, **173**, 135-184, doi: 10.1016/S1381-1169(01)00149-2.
[7] S. B. Lundin, A. Ikeda, Y. Hasegawa, Optimizing the hydrogen productivity of an ammonia decomposition membrane reactor through offset positioning of the membrane and catalyst, *Journal of Membrane Science*, 2025, **725**, 124020, doi: 10.1016/j.memsci.2025.124020.
[8] Y. Zhao, M. Sun, X. Wang, C. Wang, D. Lu, W. Ma, S. A. Kube, J. Ma, M. Elimelech, Janus electrocatalytic flow-through membrane enables highly selective singlet oxygen production, *Nature Communications*, 2020, **11**, 6228, doi: 10.1038/s41467-020-20071-w.
[9] R. B. del Olmo, M. Torres, J. Nieto-Sandoval, M. Munoz, Z. M. de Pedro, J. A. Casas, Precious metal-based Catalytic Membrane Reactors for continuous flow catalytic hydrodechlorination, *Journal of Environmental Chemical Engineering*, 2024, **12**, 112754, doi: 10.1016/j.jece.2024.112754.
[10] T. Westermann, N. Kopriwa, A. Schröder, T. Melin, Effective dispersion model for flow-through catalytic membrane reactors combining axial dispersion and pore size distribution, *Chemical Engineering Science*, 2010, **65**, 1609-1615, doi: 10.1016/j.ces.2009.10.023.
[11] V. T. Zaspalis, W. Van Praag, K. Keizer, J. G. Van Ommen, J. R. H. Ross, A. J. Burggraaf, Reactions of methanol over alumina catlytically active membranes modified by silver, *Applied catalysis*, 1991, **74**(2), 205–222.
[12] M. Kobayashi, J. Togawa, T. Kanno, J.-I. Horiuchi, K. Tada, Comparing kinetic design of propene partial oxidation between a Cs–Ag and a Re–Ag immobilized membrane reactors, *Desalination*, 2002, **144**, 399-403, doi: 10.1016/S0011-9164(02)00350-8.
[13] D. Fritsch, I. Randjelovic, F. Keil, Application of a forced-flow catalytic membrane reactor for the dimerisation of isobutene, *Catalysis Today*, 2004, **98**, 295-308, doi: 10.1016/j.cattod.2004.07.043.
[14] C. R. F. Lund, Improving selectivity during methane partial oxidation by use of a membrane reactor, *Catalysis Letters*, 1992, **12**, 395-403, doi: 10.1007/BF00765070.
[15] W. Shi, B. He, Y. Cao, J. Li, F. Yan, Z. Cui, Z. Zou, S. Guo, X. Qian, Continuous esterification to produce biodiesel by SPES/PES/NWF composite catalytic membrane in flow-through membrane reactor: Experimental and kinetic studies,

Bioresource Technology, 2013, **129**, 100-107, doi: 10.1016/j.biortech.2012.10.039.
[16] A. Schmidt, A. Wolf, R. Warsitz, R. Dittmeyer, D. Urbanczyk, I. Voigt, G. Fischer, R. Schomäcker, A pore-flow-through membrane reactor for partial hydrogenation of 1, 5-cyclooctadiene, *AIChE Journal*, 2008, **54**, 258-268, doi: 10.1002/aic.11379.
[17] C. Regmi, S. Lotfi, J. C. Espíndola, K. Fischer, A. Schulze, A. I. Schäfer, Comparison of photocatalytic membrane reactor types for the degradation of an organic molecule by TiO_2-coated PES membrane, *Catalysts*, 2020, **10**, 725, doi: 10.3390/catal10070725.
[18] J. Miao, J. Lu, H. Jiang, Y. Liu, W. Xing, X. Ke, R. Chen, Continuous and complete conversion of high concentration *p*-nitrophenol in a flow-through membrane reactor, *AIChE Journal*, 2019, **65**, e16692, doi: 10.1002/aic.16692.
[19] C. Chen, L. Lu, L. Fei, J. Xu, B. Wang, B. Li, L. Shen, H. Lin, Membrane-catalysis integrated system for contaminants degradation and membrane fouling mitigation: A review, *Science of the Total Environment*, 2023, **904**, 166220, doi: 10.1016/j.scitotenv.2023.166220.
[20] M. Reif, R. Dittmeyer, Porous, catalytically active ceramic membranes for gas–liquid reactions: a comparison between catalytic diffuser and forced through flow concept, *Catalysis Today*, 2003, **82**, 3-14, doi: 10.1016/S0920-5861(03)00197-4.
[21] F. García-Ochoa, A. Romero, The dead zone in a catalyst particle for fractional-order reactions, *AIChE Journal*, 1988, **34**, 1916-1918, doi: 10.1002/aic.690341120.
[22] A. Spence, D. J. Worth, S. T. Kolaczkowski, The treatment of non-integer exponents in reaction rate expressions, *Computers & Chemical Engineering*, 1995, **19**, 1169-1171, doi: 10.1016/0098-1354(94)00112-X.
[23] M. Szukiewicz, E. Chmiel-Szukiewicz, K. Kaczmarski, A. Szałek, Dead zone for hydrogenation of propylene reaction carried out on commercial catalyst pellets, *Open Chemistry*, **17**, 295-301, doi: 10.1515/chem-2019-0037.
[24] M. Temkin, Diffusion effects during the reaction on the surface pores of a spherical catalyst particle, *Kinetics and Catalysis*, 1975, **16**, 104–112.
[25] V. V. Andreev, Formation of a “dead zone” in porous structures during processes that proceeding under steady-state and unsteady-state conditions, *Review Journal of Chemistry*, 2013, **3**, 239-269, doi: 10.1134/s2079978013030011.
[26] P. Skrzypacz, V. V. Andreev, B. Golman, Dead-core and non-dead-core solutions to diffusion-reaction problems for catalyst pellets with external mass transfer, *Chemical Engineering Journal*, 2020, **385**, 123927, doi: 10.1016/j.cej.2019.123927.
[27] P. Skrzypacz, A. Kadyrbek, B. Golman, V. V. Andreev, Dead-core solutions to fast diffusion–reaction equation for catalyst slabs with power-law reaction kinetics and external mass transfer resistance, *Chemical Engineering Journal*, 2022, **446**, 136722, doi: 10.1016/j.cej.2022.136722.
[28] M. A. Islam, B. Ehiraj, C. K. Cheng, B. N. Dubey, M. M. R. Khan, Biofilm re-vitalization using hydrodynamic shear stress for stable power generation in microbial fuel cell, *Journal of Electroanalytical Chemistry*, 2019, **844**, 14-22, doi: 10.1016/j.jelechem.2019.05.013.
[29] F. M. Pereira, S. C. Oliveira, Occurrence of dead core in catalytic particles containing immobilized enzymes: analysis for the Michaelis–Menten kinetics and assessment of numerical methods, *Bioprocess and Biosystems Engineering*, 2016, **39**, 1717-1727, doi: 10.1007/s00449-016-1647-0.
[30] Q. Abbas, B. Golman, P. Skrzypacz, Modeling and numerical analysis for cylindrical flow-through catalytic membrane reactor with power-law reaction kinetics: Revealing dead-core phenomena, *Chemical Engineering Science*, 2024, **297**, 120283, doi: 10.1016/j.ces.2024.120283.
[31] S. Thomas, C. Hamel, A. Seidel-Morgenstern, Membrane Reactors: Distributing Reactants to Improve Selectivity and Yield, Wiley Online Library, 2010, Ch. Basic problems of chemical reaction engineering and potential of membrane reactors, pp. 1–27.
[31] S. Thomas, C. Hamel, A. Seidel-Morgenstern, Basic problems of chemical reaction engineering and potential of membrane reactors, 2010, doi: 10.1002/9783527629725.ch1.
[32] M. Menaka, R. Manimaran, S. Saravanakumar, L. Rajendran, A. Eswari, Analyzing dead core formation in catalyst pellets of various geometries under non-isothermal conditions, *Partial Differential Equations in Applied Mathematics*, 2025, **13**, 101092, doi: 10.1016/j.padiff.2025.101092.
[33] A. Haider, M. S. Anwar, Y. Nie, T. Muhammad, Numerical simulations of heat and mass transfer in Sutterby fluid within porous media using Caputo fractional derivative, *International Communications in Heat and Mass Transfer*, 2025, **164**, 108850, doi: 10.1016/j.icheatmasstransfer.2025.108850.
[34] D. Kumar, J. Singh, K. Tanwar, D. Baleanu, A new fractional exothermic reactions model having constant heat source in porous media with power, exponential and Mittag-Leffler laws, *International Journal of Heat and Mass Transfer*, 2019, **138**, 1222-1227, doi: 10.1016/j.ijheatmasstransfer.2019.04.094.
[35] M. Naeem, N. H. Aljahdaly, R. Shah, W. Weera, The study of fractional-order convection-reaction-diffusion equation *via* an Elzake Atangana-Baleanu operator, *AIMS Mathematics*, 2022, **7**, 18080-18098, doi: 10.3934/math.2022995.
[36] S. Kazbek, A. Kabiyeva, V. V. Andreev, P. Skrzypacz, B. Golman, Catalyst pellets with Gaussian activity distribution under forced periodic operation for reactions with Langmuir-Hinshelwood kinetics, *Chemical Engineering Science*, 2025, **302**, 120945, doi: 10.1016/j.ces.2024.120945.
[37] R. Aris, *The Mathematical Theory of Diffusion and Reaction in Permeable Catalysts: The theory of the steady state*, Oxford Studies in Physics Series, Clarendon Press, 1976. URL https://books.google.com.pk/books?id=aT1RAAAAMAAJ
[38] V. V. Andreev, P. Skrzypacz, B. Golman, The formation of dead zones in nonisothermal porous catalyst with temperature-dependent diffusion coefficient, *International Journal of Chemical Kinetics*, 2019, **51**, 711-722, doi: 10.1002/kin.21302.
[39] B. Golman, V. V. Andreev, P. Skrzypacz, Dead-core

solutions for slightly non-isothermal diffusion-reaction problems with power-law kinetics, *Applied Mathematical Modelling*, 2020, **83**, 576-589, doi: 10.1016/j.apm.2020.03.016.
[40] K. R. Fowler, C. T. Kelley, Pseudo-transient continuation for nonsmooth nonlinear equations, *SIAM Journal on Numerical Analysis*, 2005, **43**, 1385-1406, doi: 10.1137/s0036142903431298.
[41] X. Chen, A superlinearly and globally convergent method for reaction and diffusion problems with a non-lipschitzian operator, Topics in Numerical Analysis, Vienna, *Springer Verlag*, 2001, **15**, 79-90, doi: 10.1007/978-3-7091-6217-0_7.
[42] A. K. Aziz, A. B. Stephens, M. Suri, Numerical methods for reaction-diffusion problems with non-differentiable kinetics, *Numerische Mathematik*, 1988, **53**, 1-11, doi: 10.1007/BF01395875.
[43] J. W. Barrett, R. M. Shanahan, Finite element approximation of a model reaction: diffusion problem with a non-Lipschitz nonlinearity, *Numerische Mathematik*, 1991, **59**, 217-242, doi: 10.1007/BF01385777.
[44] F. J. Valdes-Parada, M. Sales-Cruz, J. Alberto Ochoa-Tapia, J. Alvarez-Ramirez, On Green's function methods to solve nonlinear reaction–diffusion systems, *Computers & Chemical Engineering*, 2008, **32**, 503-511, doi: 10.1016/j.compchemeng.2007.03.013.
[45] J. Solsvik, S. Tangen, H. A. Jakobsen, Evaluation of weighted residual methods for the solution of the pellet equations: The orthogonal collocation, Galerkin, tau and least-squares methods, *Computers & Chemical Engineering*, 2013, **58**, 223-259, doi: 10.1016/j.compchemeng.2013.07.002.
[46] P. Skrzypacz, N. Chalkarova, B. Golman, V. Andreev, F. Schieweck, Numerical simulations of dead zone formation in the catalytic flow-through membrane reactor, *Computers & Chemical Engineering*, 2021, **152**, 107368, doi: 10.1016/j.compchemeng.2021.107368.
[47] V. V. Andreev, P. Skrzypacz, B. Golman, Taylor series solutions to steady-state non-isothermal diffusion–reaction problems for porous catalyst pellets with arbitrary kinetics, *Mathematical Methods in the Applied Sciences*, 2024, **47**, 1514-1545, doi: 10.1002/mma.9699.
[48] P. G. Ciarlet, *Linear and Nonlinear Functional Analysis with Applications*. Philadelphia, PA: Society for Industrial and Applied Mathematics, 2013 doi: 10.1137/1.9781611972597.
[49] D. H. Griffel, *Applied Functional Analysis*, ELLIS HORWOOD LIMITED, 2002, 390, ISBN - 9780486422589
[50] G. D. Smith, *Numerical Solution of Partial Differential Equations: Finite Difference Methods*, Clarendon Press, 1985, 337, ISBN- 9780198596509